Energy, exergy and environmental assessment of a cascade refrigeration system with internal heat exchanger based on eco-friendly refrigerants

Malek Hamzaoui[1], Samir Tiachacht[1*], Ali Grine[3], Ahmed Hadiouche[2]

[1] Laboratory of Mechanics, Structure and Energetics (LMSE), Mouloud Mammeri University of Tizi-Ouzou, Algeria
[2] Laboratory of Energetic, Mechanics and Material (LEMM), Mouloud Mammeri University of Tizi-Ouzou, Algeria
[3] Mechanical Engineering Department, M'hamed Bougara University of Boumerdes, Boumerdes, Algeria
[*]Corresponding author: samir.tiachacht@ummto.dz

ARTICLE INFO

DOI:10.46223/HCMCOUJS.asc.en.16.1.80.2026

Received: January 09th, 2026

Revised: April 29th, 2026

Accepted: May 04th, 2026

Keywords:

cascade refrigeration system; COP; environmental analysis; exergy analysis; optimization; TEWI

ABSTRACT

Very low-temperature refrigeration is required in several applications, including cryogenics, pharmaceutical preservation, and ultra-low-temperature freezing. However, achieving such conditions with conventional single-stage systems is difficult because of the high compression ratios involved and the resulting energy losses. In this study, two pairs of environmentally friendly refrigerants with low Global Warming Potential (GWP), namely R744/R290 and R744/R152a, were investigated in a laminar refrigeration system equipped with an internal heat exchanger. A comprehensive parametric analysis was conducted to determine the optimal operating conditions for evaporation temperatures from -55°C to -25°C and condensation temperatures from 25°C to 60°C. The Quadratic Interpolation Optimization (QIO) method was used to determine the optimal intermediate temperature, $T_{4H,opt}$, for enhancing energy efficiency, exergy performance, and environmental sustainability. The results show that, under all condensing conditions, R744/R290 is more advantageous at very low evaporation temperatures from both thermodynamic and environmental perspectives. Meanwhile, R744/R152a provides better overall performance when the evaporation temperature is ≥ -30°C.

1. Introduction

The refrigeration industry is currently facing a dual challenge: meeting rapidly growing global cooling demand while minimizing environmental impact and energy consumption. To address this challenge, improving energy efficiency and decarbonization in refrigeration systems has been attracting scientists. Among the available technologies, including mechanical compression (Adebayo et al., 2021), absorption (Liu et al., 2022), and emerging ejector-based systems (Bencharif et al., 2020; Hamzaoui et al., 2018), the vapor-compression cycle remains the dominant solution, owing to its technological maturity, superior performance, and high

flexibility in refrigerant selection (de Paula et al., 2020; Kilicarslan & Hosoz, 2010; Kumar et al., 2024, 2026). However, this dominance comes with a significant energy cost, such as according to the International Institute of Refrigeration (IIR), the refrigeration and air-conditioning sector accounted for nearly 20% of global electricity consumption in 2019 (Lizarte et al., 2017). Therefore, the IIR recognizes energy efficiency optimization as a major environmental priority for the sector (Lizarte et al., 2017). To adopt this challenge, two complementary strategies are evolving. The first involves harnessing non-electrical energy sources such as solar, geothermal, or industrial waste heat (Davoodi et al., 2022; Han et al., 2007; Salhi et al., 2018) to reduce reliance on the electrical grid and decarbonize cooling production. Another important solution is the use of more sustainable refrigerants, with natural refrigerants increasingly being seen as viable alternatives. Carbon dioxide (R744) is considered suitable for low-temperature refrigeration systems due to its favorable environmental properties, including zero ozone depletion potential (ODP = 0) and very low global warming potential, with a GWP of only 1 (Hamzaoui, Aidoun, et al., 2024). Although CO_2 operates at relatively high pressures, which can present some technical challenges, this characteristic is advantageous in low-temperature applications. However, CO_2's relatively low critical temperature of only 31.1°C can reduce system efficiency in hot conditions (Lemmon et al., 2007). To deal with these limitations, recent studies have focused on advanced thermodynamic configurations, particularly cascade refrigeration systems, with Nesreddine et al. (2015) developed a CO_2/R245fa prototype in which a supersonic ejector drives the high-temperature cycle, enabling CO_2 condensation at approximately 20°C. Hybrid approaches combining absorption and compression have also been proposed by Gado et al. (2022). Concurrently, comparative studies have evaluated numerous refrigerant pairs: Kilicarslan and Hosoz (2010) analyzed R123 in the low-temperature loop paired with various high-temperature refrigerants, while Bhattacharyya et al. (2009) achieved -65°C using nitrous oxide (R744A). Sun et al. (2016) and Sun et al. (2019) demonstrated that an R23-based cycle can reach as low as -83°C, and Logesh et al. (2019) identified optimal candidates for -70°C applications. More recently, Hamzaoui, Aidoun, et al. 2024 showed that the R744/R1270 pair delivers the best performance among five tested natural refrigerant combinations. Recent experimental and simulation studies further reinforce this trend, showing that efficient refrigeration system design requires a combination of stable refrigerants, optimal configuration, and appropriate control of operating parameters. Udroiu et al. (2025) displayed that the hydrocarbon pair R290/R170 significantly betters than conventional HFCs (R404A/R23), achieving a COP of 0.95, a reduced discharge temperature (~50°C), and a 50% reduction in CO_2-equivalent emissions (via TEWI analysis). Ye et al. (2026) optimized a similar system using the MOGWO algorithm, attaining minimal exergy destruction (32.08W, i.e., -50.8%), an optimal inter-stage capacity ratio (ICR = 0.23), and a controlled annual economic cost of $4,015.90/year. Meanwhile, Ma et al. (2025) highlighted the critical role of refrigerant charge: a 300g overcharge increases power consumption by 4.9 - 9.0% while degrading COP by 3.25 - 5.77%, justifying a +5 - 10% adjustment above the theoretical optimum to compensate for leaks and aging. Finally, Pektezel and Ozdemir (2025) optimized a three-stage cycle using response surface methodology, achieving a COP of 0.697 and an exergetic efficiency of 41.4% at -90°C.

Previous studies on cascade refrigeration systems have mainly focused on thermodynamic performance analysis and optimization. However, their environmental impacts have received relatively limited attention. Overall, recent studies tend to reach a similar conclusion: sustainable refrigeration will depend on the combined use of natural refrigerants, optimization methods, and

proper control of operating conditions. These three factors, namely performance, sustainability, and reliability, provide an important basis for developing the next generation of refrigeration systems. Such systems are expected to meet very low-temperature requirements while also reducing energy consumption and carbon emissions in response to current climate challenges.

2. Modelling

The thermodynamic model was developed based on several assumptions. First, the system was assumed to operate under steady-state conditions. Pressure drops in the piping and components were neglected, and changes in kinetic and potential energy were considered insignificant. The refrigerants were assumed to leave all heat exchangers in a saturated state, while the expansion processes through the valves were treated as isenthalpic. In addition, the separation/mixing vessels and the cascade heat exchanger were considered perfectly insulated, or adiabatic. A constant temperature pinch of $\Delta T = T_{3L} - T_{4H} = 5℃$ was imposed in the evaporator condenser (Hamzaoui, Aidoun, et al., 2024). The environmental reference conditions are defined as $p_0 = 1.01325\ bar$ (1atm) and $T_0 = 25℃$ (298.15 K) (Hamzaoui, Aidoun, et al., 2024).

2.1. Working fluids

This work considers environmentally friendly refrigerants with low Global Warming Potential (GWP) and zero ozone depletion potential (ODP). R744 (CO_2), R290 (propane), and R152a (1.1-difluoroethane) were selected due to their suitable thermodynamic properties and low environmental impact. As shown in Table 1, all three refrigerants have a GWP below 150, meeting current international regulations such as the Kigali Amendment and the EU F-Gas policy.

R744 is used for Low-Temperature Cycles (LTC) due to its good heat transfer and high volumetric cooling capacity, even at relatively high operating pressures. In high-temperature cycles (HTC), R290 and R152a are chosen as alternative refrigerants; R290 has a low GWP of 5 but is highly flammable, while R152a has a GWP of 124 and is only slightly flammable. Despite having negligible ODPs, R290 and R152a differ in flammability and thermophysical properties, potentially resulting in differences in system performance under harsh conditions. Therefore, this choice helps balance performance, safety, and environmental sustainability.

Table 1

Thermophysicals Properties

Fluid	Chemical formula	Molecular weight	GWP	ODP	Pc [bar]	Tc [°C]	NBT [°C]	Safety class
R744 (Hamzaoui, Aidoun, et al., 2024)	CO_2	44.01	1	0	73.773	30.98	-78.46	A1
R152a (Cabello et al., 2017)	$C_2H_4F_2$	66.051	124	0	45.168	113.26	-24.02	A2
R290 (Hamzaoui, Tiachacht, & Hadiouche, 2024)	C_3H_8	44.096	5	0	42.512	96.74	-42.11	A3

Note. Compiled by the authors

2.2. System description

The cascade refrigeration system investigation in this study consists of two thermally coupled single-stage vapour-compression cycles: a Low-Temperature Cycles (LTC) and a High-Temperature Cycle (HTC), interconnected via a cascade heat exchanger that acts simultaneously as the condenser for the LTC and the evaporator for the HTC. A simplified schematic of the system is presented in Figure 1, while the corresponding temperature-entropy (T-s) diagram is shown in Figure 2.

In the LTC, carbon dioxide (R744) is employed due to its excellent thermodynamic properties at very low temperatures and its negligible environmental impact (GWP = 1, ODP = 0). The HTC operates with either propane (R290) or 1.1-difluoroethane (R152a), both low-GWP, natural or mildly flammable alternatives that comply with current environmental regulations.

The refrigeration load QE is absorbed in the evaporator of the LTC (process 4L → 1L). The vapor leaving the evaporator then passes through an internal heat exchanger (IHXLTC), where it is superheated before entering the LTC compressor (1sL → 2L). The high-pressure, superheated vapour is subsequently condensed in the cascade heat exchanger (2L → 3L), releasing heat to the HTC. The liquid refrigerant is further subcooled in the IHXLTC (3L → 3rL) before undergoing isenthalpic expansion through the expansion valve (3rL → 4L), completing the LTC loop. Similarly, in the HTC, the refrigerant evaporates in the cascade heat exchanger (4H → 1H), absorbing the heat rejected by the LTC. It is then superheated in the internal heat exchanger (IHXHTC) (1H → 1sH) before being compressed (1sH → 2H). The hot discharge vapour rejects heat to the ambient in the condenser (2H → 3H), is subcooled in the IHXHTC (3H → 3rH), and finally expanded isenthalpically (3rH → 4H) to close the cycle.

Figure 1

Cascade Refrigeration System with Internal Heat Exchanger

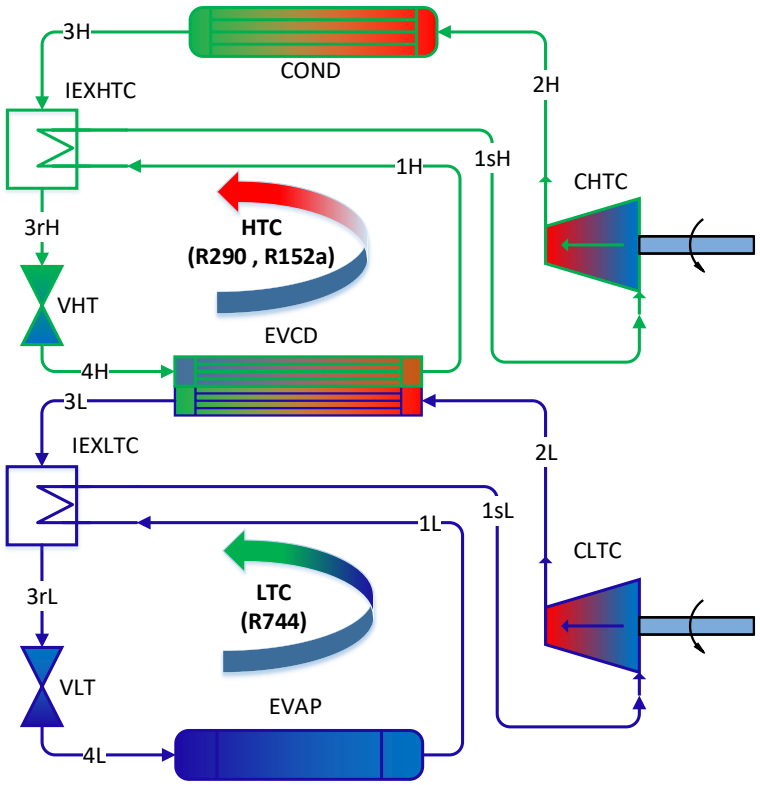

Note. Compiled by the authors

The arrangement of the heat exchangers in both cycles improves system efficiency by increasing the degree of supercooling and superheating, thereby reducing compression work and improving the Coefficient of Performance (COP). The entire system is assumed to operate in a steady state, with perfect insulation for all equipment except the evaporator, condenser, and cascaded heat exchangers.

Figure 2

T-s Diagram

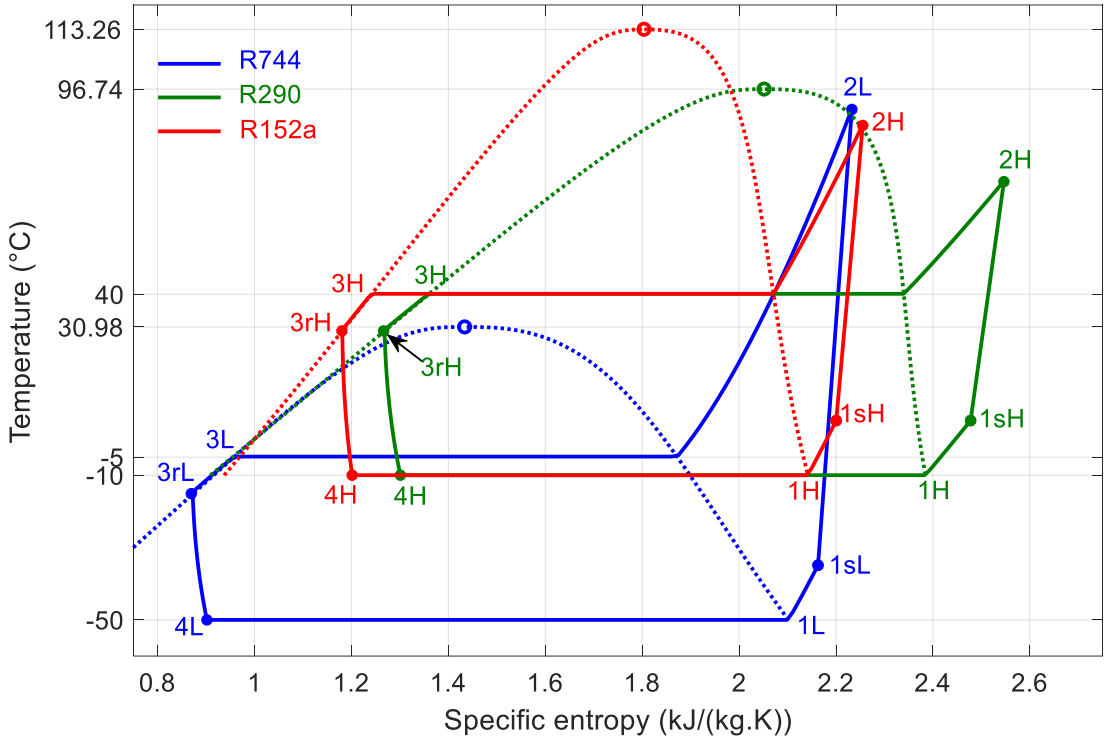

Note. Compiled by the authors

2.3. Methodology

The thermodynamic efficiency of cascaded refrigeration systems is evaluated by energy and exergy analysis based on the first and second laws of thermodynamics, in which the total power consumption of the compressors is determined as follows:

$$\dot{W} = \dot{W}_{LT} + \dot{W}_{HT} \tag{1}$$

With $$\dot{W}_{LT} = \dot{m}_{LT}(h_{2L} - h_{1sL}) \tag{2}$$

and $$\dot{W}_{HT} = \dot{m}_{HT}(h_{2H} - h_{1sH}) \tag{3}$$

Isentropic efficiencies for the compressors are modeled as functions of the compression ratio (Hamzaoui, Aidoun, et al., 2024):

$$\eta_{isLT} = 0.8981 - 0.092384 \times \tau_{LT} + 0.00476 \times {\tau_{LT}}^2 \tag{4}$$

$$\eta_{isHT} = 0.85 - 0.046667 \times \tau_{HT} \tag{5}$$

With $$\tau_{LT} = {P_{2L}}/{P_E} \text{ and } \tau_{HT} = {P_C}/{P_{1H}} \tag{6}$$

Energy balances for key components yield (see Table 2):

Table 2

Energy Balance

Components	Exergy	Number
Condenser	$\dot{Q}_C = \dot{m}_{HT}(h_{2H} - h_{3H})$	(7)
LTC Expansion valves	$h_{3rL} = h_{4L}$	(8)
HTC Expansion valves	$h_{3rH} = h_{4H}$	(9)
Evaporator	$\dot{Q}_E = \dot{m}_{LT}(h_{1L} - h_{4L})$	(10)
Cascade heat exchanger	$\dot{m}_{HT}(h_{1H} - h_{4H}) = \dot{m}_{LT}(h_{2L} - h_{3L})$	(11)
HTC internal heat exchangers	$h_{1sH} - h_{1H} = h_{3H} - h_{3sH}$	(12)
LTC internal heat exchangers	$h_{1sL} - h_{1L} = h_{3L} - h_{3sL}$	(13)

Note. Compiled by the authors

A system is in thermodynamic equilibrium with the environment when its temperature, pressure, and chemical potential match those of the ambient (reference) state; under these conditions, its exergy is zero (Hamzaoui, Aidoun, et al., 2024). Exergy analysis is used to identify losses and improve energy system design. In this study, this method is applied to a cascaded refrigeration system to identify the components with the highest levels of irreversibility through the calculation of exergy losses and exergy efficiency, thereby highlighting key areas for efficiency improvement. It can be seen that from Figures 1 and 2 and Table 3, the exergy destruction rates of the system components are formulated under the assumptions that changes in kinetic and potential energy are negligible and that the ambient temperature T_0 is taken as the reference state.

Table 3

Exergy Destruction

Components	Exergy destruction	Number
LT compressor	$\dot{X}_{LT} = \dot{m}_{LT}T_0(s_{2L} - s_{1sL})$	(14)
HT compressor	$\dot{X}_{HT} = \dot{m}_{LT}T_0(s_{2H} - s_{1sH})$	(15)
Condenser	$\dot{X}_C = \dot{m}_{HT}[h_{2H} - h_{3H} - T_0(s_{2H} - s_{3H})] - \dot{Q}_C\left(1 - \frac{T_0}{T_C}\right)$	(16)
LT expansion valve	$\dot{X}_{VLT} = \dot{m}_{LT}T_0(s_{4L} - s_{3rL})$	(17)
HT expansion valve	$\dot{X}_{VHT} = \dot{m}_{HT}T_0(s_{4H} - s_{3rH})$	(18)
Evaporator	$\dot{X}_E = \dot{m}_{LT}[h_4 - h_1 - T_0(s_4 - s_1)] + \left[\dot{Q}_E\left(1 - \frac{T_0}{T_E + \Delta T}\right)\right]$	(19)
IEXLTC	$\dot{X}_{IESLT} = \dot{m}_{LT}T_0[(s_{1sL} - s_{1L}) + (s_{3rL} - s_{3L})]$	(20)
IEXHTC	$\dot{X}_{IESHT} = \dot{m}_{HT}T_0[(s_{1sH} - s_{1H}) + (s_{3rH} - s_{3H})]$	(21)
EVCD	$\dot{X}_{cas} = \dot{m}_{HT}T_0(s_{1H} - s_{4H}) + \dot{m}_{LT}T_0(s_{3L} - s_{2L})$	(22)

Note. Compiled by the authors

2.4. Performance

System performance is quantified using two key metrics:

An energy-based indicator, coefficient of performance (COP):

$$COP = \frac{\dot{Q}_E}{\dot{W}} \tag{23}$$

A second-law metric reflecting thermodynamic effectiveness, exergetic efficiency:

$$\eta_{ex} = 1 - \frac{\dot{X}_{SYS}}{\dot{W}} \tag{24}$$

With:

$$\dot{X}_{SYS} = \dot{X}_{LT} + \dot{X}_{HT} + \dot{X}_C + \dot{X}_{VLT} + \dot{X}_{VHT} + \dot{X}_E + \dot{X}_{cas} + \dot{X}_{IESLT} + \dot{X}_{IESHT} \tag{25}$$

2.5. Environmental impact

The environmental footprint is evaluated using the Total Equivalent Warming Impact (TEWI), which combines direct emissions (from refrigerant leakage) and indirect emissions (from electricity consumption):

$$TEWI = TEWI_{DIR} + TEWI_{IND} \tag{26}$$

$$TEWI_{DIR} = \text{GWP. m. de} + \text{GWP. m.}\,(1 - dr) \tag{27}$$

$$TEWI_{IND} = E.\beta.t.n \tag{28}$$

where:

- $m = \dot{m}_{ref} \times 240s$, is the initial refrigerant charge (Hamzaoui, Aidoun, et al., 2024),
- $de = 0.1$ (annual leakage rate) (Hamzaoui, Aidoun, et al., 2024),
- $dr = 0.9$ (recycling factor) (Hamzaoui, Aidoun, et al., 2024),
- $n = 15\ years$ (system lifetime),
- $t = 8760\ h/year$,
- $\beta = 0.503\ kg_{CO2}/kWh$ (Algerian grid emission factor in 2020).

This holistic metric ensures that environmental decisions account for both refrigerant choice and long-term energy use.

3. Model validation

The reliability of the thermodynamic model in this study was evaluated by comparing simulation results with experimental data from Cabello et al. (2017) for a cascaded refrigeration system using the R744/R152a refrigerant pair. The validation process focused on two main parameters: the discharge temperature of the high-temperature cycle compressor, T_{2H}, and the overall efficiency coefficient COP.

Table 4

Validation for R744/R152a

T_E [°C]	T_C [°C]	T_{4H} [°C]	ΔT_{cas} [°C]	COP (Cabello et al., 2017)	Present COP	Error [%]	T_{2H} [°C] (Cabello et al., 2017)	T_{2H} [°C] present	Error [%]
-30	30	-6.6	4.3	1.585	1.617	-1.36	77.9	79.97	-2.66
-35	30	-9.8	4.9	1.392	1.435	-2.96	82.4	83.27	-1.06
-40	30	-12.2	6.0	1.198	1.260	-4.9	85.1	85.84	-0.87
-30	40	-5.4	3.4	1.388	1.409	-1.47	90.2	94.45	-4.72
-35	40	-8.1	4.1	1.219	1.257	-3.06	95.7	97.15	-1.52
-40	40	-10.5	5.3	1.044	1.111	-5.99	100.6	99.63	0.97
-30	50	-3.3	3.1	1.223	1.215	0.69	100.8	107.32	-6.47
-35	50	-6.2	3.9	1.08	1.092	-1.11	106.3	110.15	-3.58
-40	50	-9.2	4.9	0.933	0.981	-4.91	111.1	113.10	-1.80

Note. Compiled by the authors

As in Table 4, it is known that the simulated results agree well with the experimental measurements across the investigated operating range, with evaporator temperatures varying from -40°C to -30°C and condenser temperatures from 30°C to 50°C. The maximum absolute deviation for the high-temperature compressor discharge temperature is no greater than 6.5%, and the difference in COP stays below 6% in all cases. The slight deviations are mainly due to the simplifying assumptions adopted in the model, such as neglecting pressure drops, assuming perfect insulation, and considering the expansion process to be isenthalpic. These assumptions may make the model slightly overestimate the system performance compared with actual operation. However, the good agreement between the simulation and experimental results shows that the proposed model is reliable. Therefore, it can be used for further parametric studies, optimization, and comparison of different refrigerant pairs under similar operating conditions.

4. Parametric study

A comprehensive parametric analysis is conducted to evaluate the influence of the intermediate evaporation temperature in the high-temperature cycle (T_{4H}) on the overall performance of the cascade refrigeration system. The study focuses on two environmentally friendly refrigerant pairs: R744/R290 and R744/R152a, with R744 (CO_2) used in the Low-Temperature Cycle (LTC) and either R290 or R152a in the High-Temperature Cycle (HTC). The system is designed to deliver a cooling capability of $\dot{Q}_E = 10kW$ at an evaporator temperature of $T_E = -40℃$, while rejecting heat at a condenser temperature of $T_C = 50℃$, demanding operating condition representative of severe ambient environments. A constant temperature pinch of $\Delta T_{cas} = 5℃$ is imposed across the cascade heat exchanger, as detailed in Table 5.

Figure 3

Influence of T_{4H} on the Compressor Discharge Temperature and Mass Flow Ratio

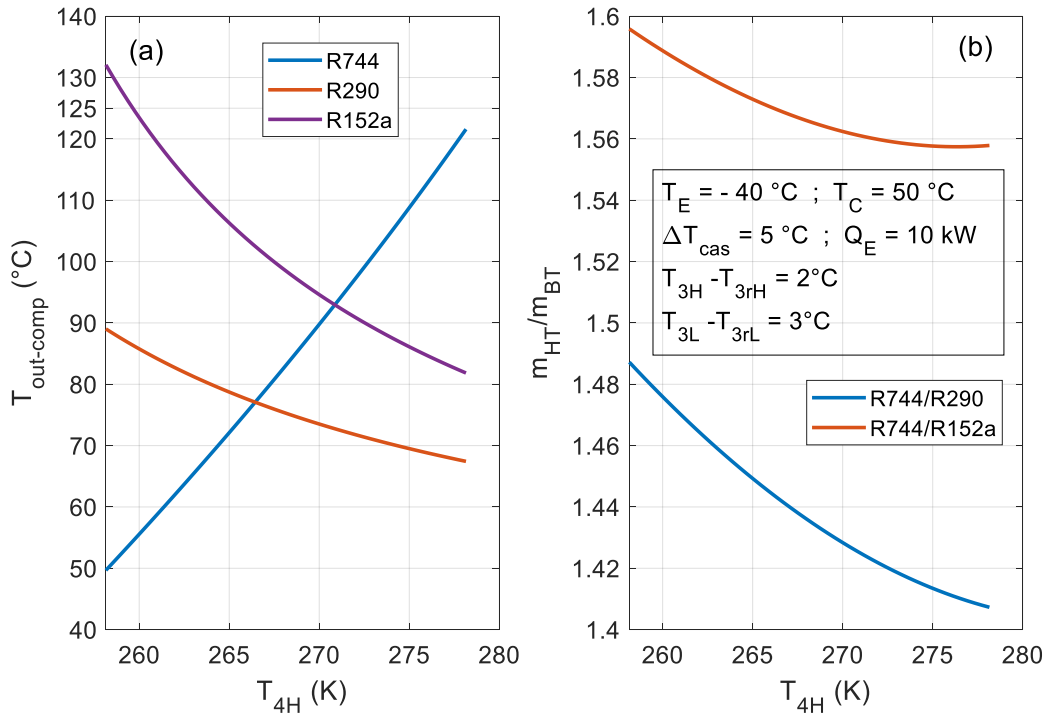

Note. Compiled by the authors

Table 5

Operation Conditions

T_E [°C]	T_C [°C]	ΔT_{cas}[°C]	ΔT_{rHT}[°C]	ΔT_{rLT}[°C]	$\dot{Q}_E$ [kW]
-40	50	5	2	3	10

Note. Compiled by the authors

Figure 3 indicates the variation trend of compressor discharge temperatures and flow rate ratios for the two considered fluid pairs. According to the simulation results presented in Figure 3a, the temperature T_{2L} increases with the increase of T_{4H} due to the increase of $\Delta T_{lift-LT}$ $\left(\Delta T_{lift-LT} = T_{3L} - T_E\right)$, hence the compression ratio of the LT loop increases, while the discharge temperature of the HT loop compressor decreases because $\Delta T_{lift-HT}$ $\left(\Delta T_{lift-HT} = T_C - T_{4H}\right)$ decreases with the increase of T_{4H}. It is noted that $T_C - T_E = \Delta T_{lift} = \Delta T_{lift-HT} + \Delta T_{lift-LT} - \Delta T_{cas}$. Consequently, Figure 3b shows the effect of T_{4H} on the flow rate ratios. From this figure, and as the cooling capacity is 10kW, the refrigerant mass flow rate of the LT loop increases with the increase of T_{4H}. Moreover, $\dot{m}_{HT}$ also increases due to the decrease in $h_{1H} - h_{4H}$. Nevertheless, the flow rate ratio $\dot{m}_{LT}/\dot{m}_{HT}$ decreases as the rate of increase of $\dot{m}_{LT}$ is higher compared to that of $\dot{m}_{HT}$.

Figure 4 shows the effect of temperature T_{4H} on exergy destruction and total power consumption. Exergy destruction and power consumed by the compressors have the same trends with temperature T_{4H}. Both quantities (W and X) decrease and then increase with the increase of the intermediate temperature T_{4H} of the cascade system. It is noted that the minimum values for $\dot{W}$ and $\dot{X}$ are located at the same T_{4H}.

Figure 4

Influence of T_{4H} on the Exergy Destruction and Compressor Consumption

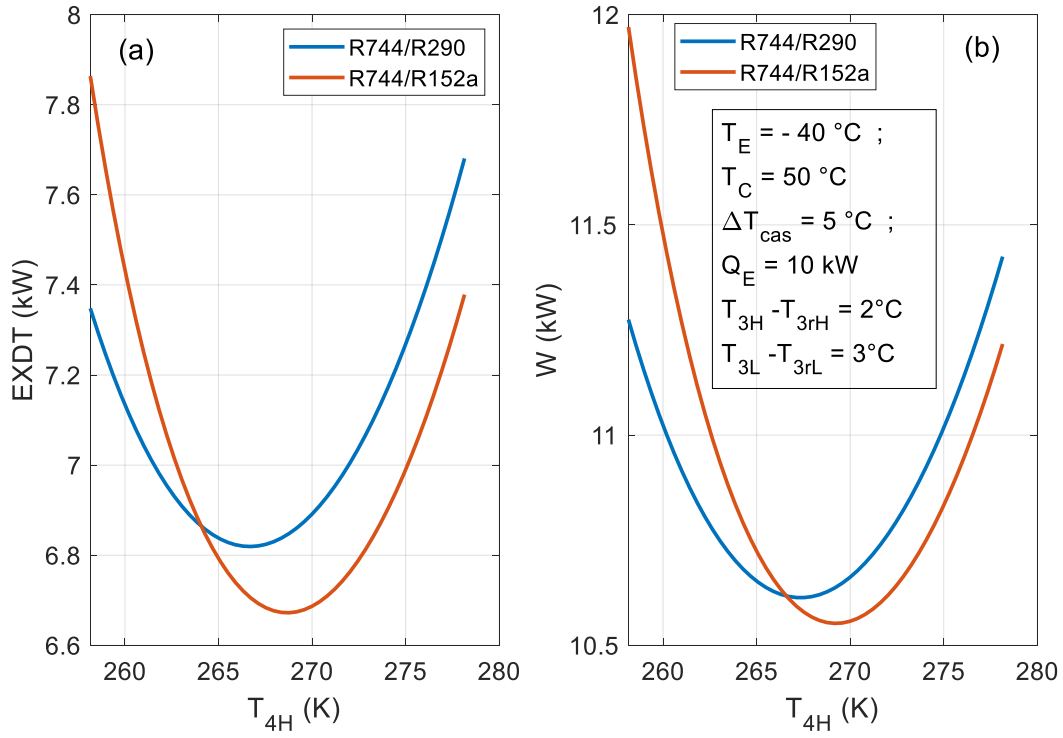

Note. Compiled by the authors

Figure 5 presents the variation of the Coefficient of Performance (COP) and the exergetic efficiency as a function of the intermediate temperature T_{4H} (i.e., the evaporation temperature in the high-temperature cycle, which also corresponds to the condensation temperature in the low-temperature cycle), for the specified operating conditions and refrigerant pairs. In this configuration, the Low-Temperature Cycle (LTC) operates with R744 (CO_2), while the High-Temperature Cycle (HTC) uses either R290 or R152a. For each refrigerant pair, COP reaches its maximum value at the optimal intermediate temperature of the cascaded system, T_{4H}, which lies within a narrow range of 265K to 270K. This optimal value varies slightly depending on the refrigerant used in the High-Temperature Cycle (HTC), due to differences in thermophysical properties and compatibility between the two cascaded cycles. Among the studied pairs, R744/R152a provides the highest COP across the investigated range, showing better energetic performance than R744/R290 under the same conditions.

This figure also shows that as the total compressor power decreases, both COP and exergy efficiency increase and reach a maximum at the same optimal T_{4H} value, indicating lower exergy losses and improved thermodynamic efficiency. Consistently, the R744/R152a configuration yields the highest exergetic efficiency, reinforcing its advantage not only from an energy standpoint but also from a second-law perspective.

Figure 5

Influence of T_{4H} on the COP and Exergy Efficiency

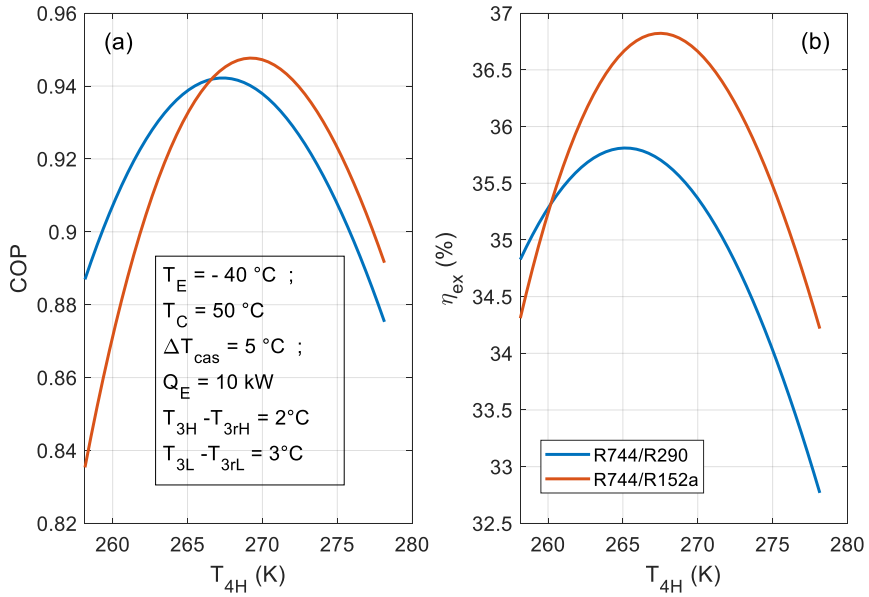

Note. Compiled by the authors

Figure 6

Influence of T_{4H} on the TEWI

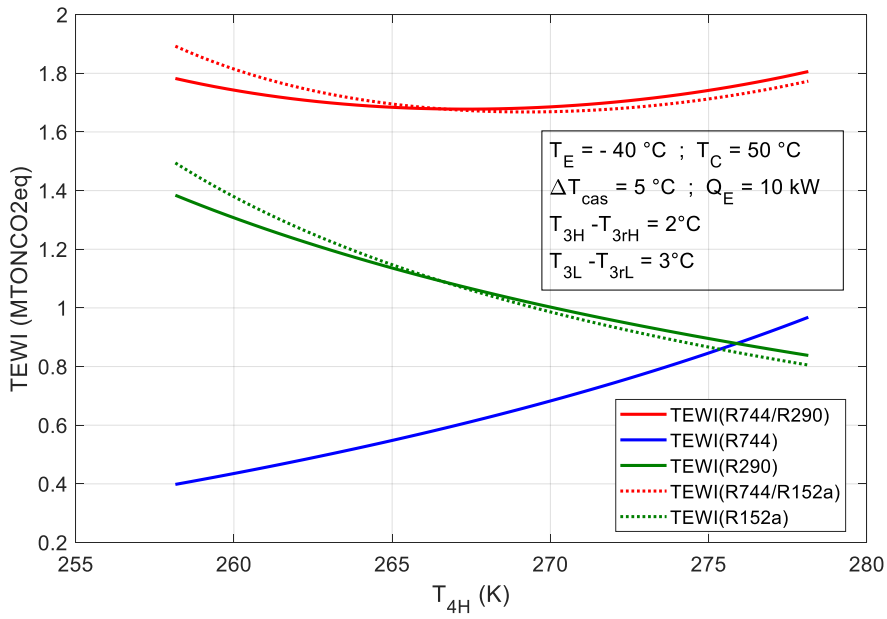

Note. Compiled by the authors

Figures 6 and 7 illustrate the variation of the TEWI as a function of the T_{4H}. An increase in T_{4H} leads to higher power consumption in the LT compressor, which consequently increases the indirect component of the TEWI (CO_2), while the power consumed by the HT compressor decreases with the increase in T_{4H} as $\Delta T_{lift-HT}$ decreases, causing the decrease in TEWI(HT). Moreover, for $T_{4H} = 266.6K$, $TEWI(R290) = TEWI(R152a)$, despite the different GWPs, this temperature shows a very remarkable value that gives the pair used for each interval $T_{4H} > 266.6K$ and $T_{4H} < 266.6K$. Additionally, the minimum of global TEWI is marked at $T_{4H} = 267.5K$ for the R744/R290 pair and at $T_{4H} = 269.3K$ for the R744/R152a pair.

Figure 7

Influence of T_{4H} on the Direct and Indirect TEWI

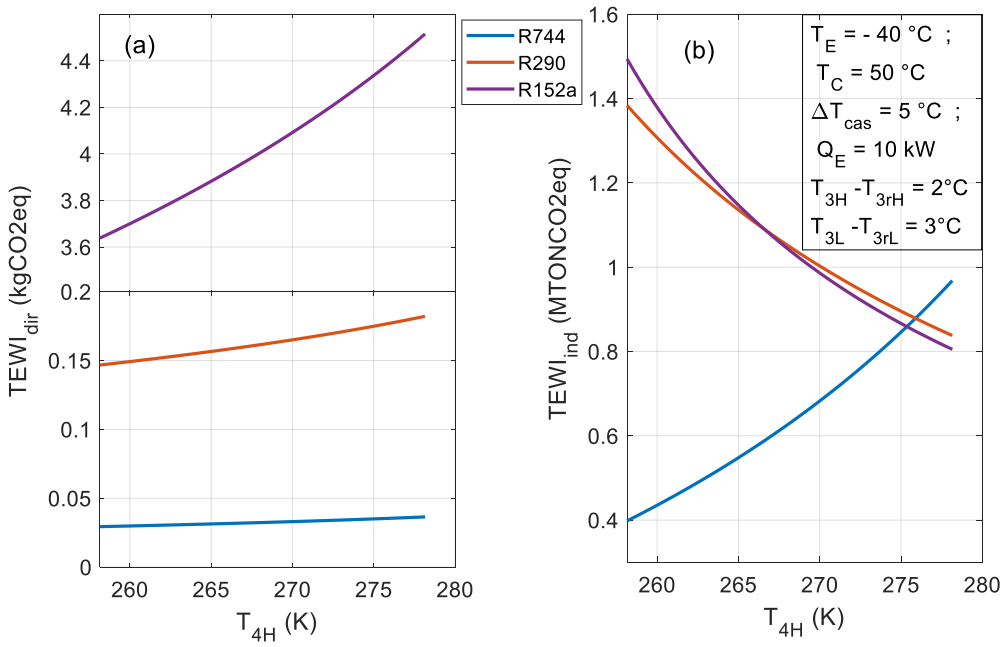

Note. Compiled by the authors

Figure 7 shows the variations of direct and indirect TEWI. The direct TEWI is practically negligible compared to the indirect TEWI. According to Figure 7a, it is observed that $TEWI_{DIR}(R744) < TEWI_{DIR}(R290) < TEWI_{DIR}(R152a)$ because $GWP(R744) < GWP(R290) < GWP(R152a)$. On the other hand, Figure 7b shows the variation of indirect TEWI, this variation is directly linked to the electrical power consumed by each compressor for the considered lifetime.

5. Optimization method

5.1. Objective function

The optimization of the considered installation is based on minimizing the objective function defined as follows:

$$f(T_E, T_C, \Delta T_{CAS}, COP) = COP - COP_C \tag{29}$$

$$min\big(f(T_E, T_C, \Delta T_{CAS}, COP)\big) = min(COP - COP_C) \tag{30}$$

With: $T_{4H,min} \leq T_{4H} \leq T_{4H,max}$ and $COP_C = \frac{T_E}{T_C - T_E}$ (31)

5.2. Choice of optimization method

To ensure optimal system performance, appropriate optimization techniques must be applied to determine the most favourable operating conditions. In this study, several methods were tested to identify the method best suited for the considered refrigeration system. Namely, the QIO method (Quadratic Interpolation Optimization) (Zhao et al., 2023), the Puma method (Abdollahzadeh et al., 2024), the ALO method (Mirjalili, 2015), and the LCA method (Houssein et al., 2023).

Figure 8

Fitness vs Iteration

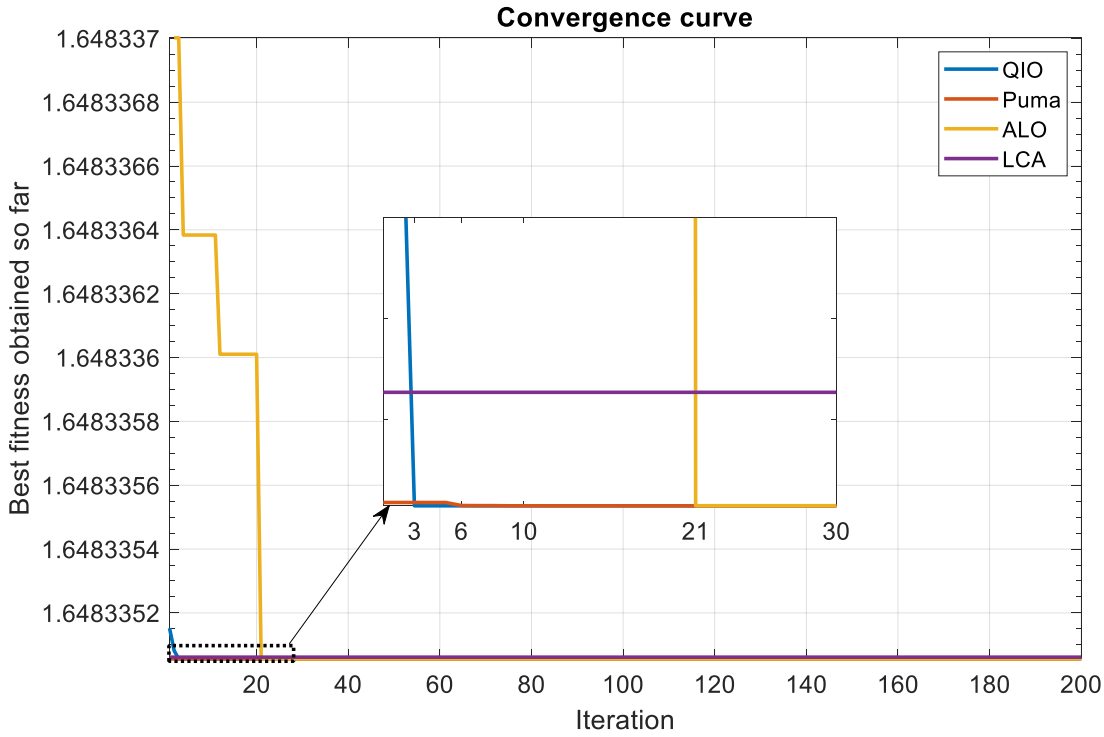

Note. Compiled by the authors

Figure 9

Best Solution vs Optimization Method

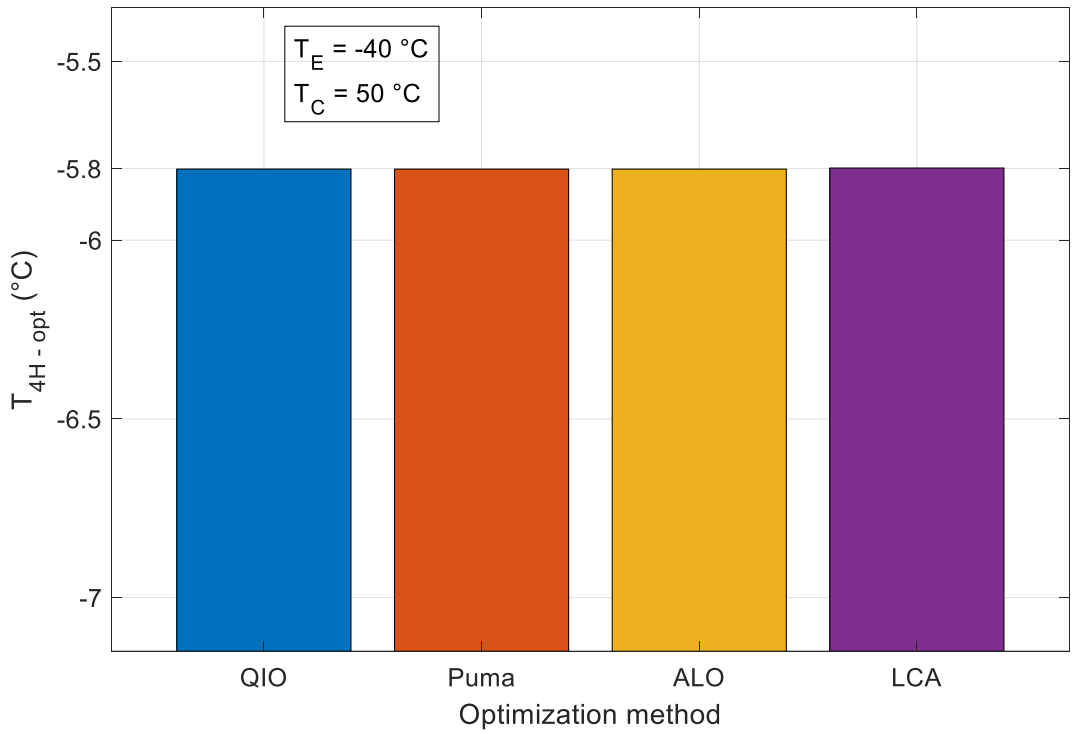

Note. Compiled by the authors

Figure 10

Flowchart of QIO

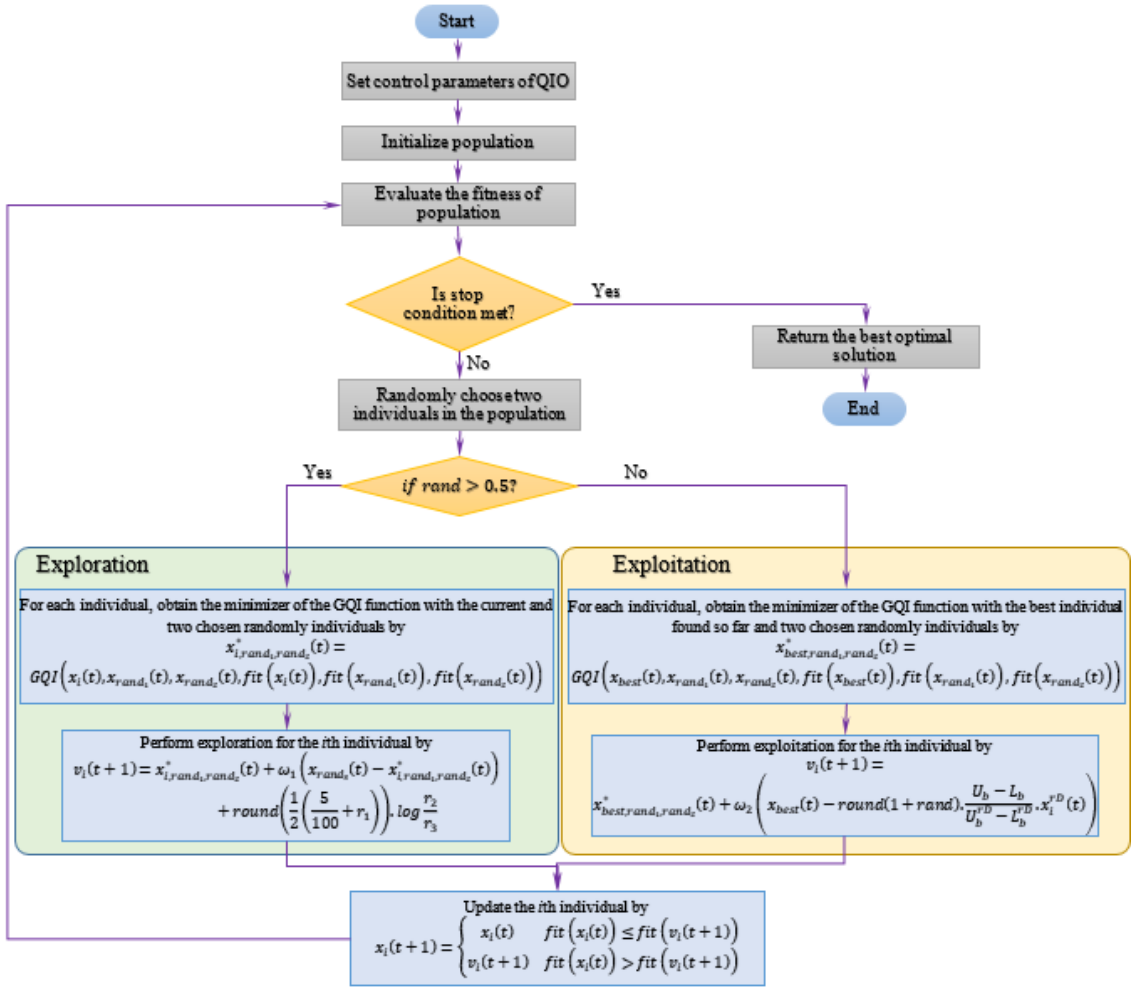

Note. Compiled by the authors

Figures 8 and 9 show the convergence and the optimized value, respectively, for 200 iterations and 200 populations with $T_E = -40℃$ and $T_C = 50℃$. As shown in Figure 8 the QIO algorithm converges in only three iterations, demonstrating a faster convergence rate compared with the other optimization methods. In contrast, the others have a higher number of iterations for convergence. Therefore, and after comparison between the four methods, the QIO algorithm was selected for the optimization procedure due to its rapid convergence and improved stability. The flowchart of the method QIO is depicted in Figure 10. For further information, please refer to reference (Zhao et al., 2023).

6. Results and discussions

Tables 6 and 7 depict the variation of T_{4H} in relation to the system's evaporation and condensation temperatures with $\Delta T_{cas} = 5℃$, respectively, for the R744/R290 and R744/R152a pairs. It is observed that for a fixed evaporation temperature, $T_{4H\text{-}opt}$ increases with increasing condensation temperature, and vice versa when the condensation temperature is fixed and the evaporation temperature is increased. Moreover, $T_{4H\text{-}opt}$ also varies with the refrigerant type for any fixed evaporation and condensation temperatures. Furthermore, for any evaporation or condensation temperatures, $T_{4H\text{-}opt}$ is generally negative except for the R744/R152a pair, where for $(T_C, T_E) = (50, -30)℃$, $T_{4H\text{-}opt}$ is positive.

Table 6

Optimized T_{4H} for R744/R290 Pair

T_E \ T_C	25	30	35	40	45	50	55	60
-55	-23.84	-21.62	-19.37	-17.09	-14.76	-12.37	-9.89	-7.3
-50	-21.39	-19.21	-17.01	-14.79	-12.54	-10.25	-7.91	-5.51
-45	-18.94	-16.79	-14.63	-12.45	-10.25	-8.03	-5.77	-3.47
-40	-16.53	-14.40	-12.27	-10.13	-7.97	-5.8	-3.61	-1.38
-35	-14.14	-12.05	-9.96	-7.86	-5.74	-3.62	-1.48	0.67
-30	-11.8	-9.75	-7.7	-5.64	-3.58	-1.51	0.57	2.66
-25	-9.48	-7.49	-5.49	-3.48	-1.48	0.53	2.54	4.55

Note. Compiled by the authors

Table 7

Optimized T_{4H} for R744/R152a Pair

T_E \ T_C	25	30	35	40	45	50	55	60
-55	-20.93	-18.59	-16.24	-13.87	-11.47	-9.04	-6.54	-3.98
-50	-18.89	-16.62	-14.34	-12.06	-9.77	-7.47	-5.16	-2.83
-45	-16.83	-14.6	-12.37	-10.15	-7.94	-5.72	-3.51	-1.3
-40	-14.76	-12.57	-10.4	-8.22	-6.06	-3.91	-1.77	0.36
-35	-12.70	-10.56	-8.43	-6.31	-4.2	-2.11	-0.03	2.03
-30	-10.66	-8.56	-6.48	-4.41	-2.36	-0.322	1.69	3.68
-25	-8.62	-6.58	-4.55	-2.54	-0.55	1.41	3.36	5.28

Note. Compiled by the authors

Figure 11

Cop Ration Optimized

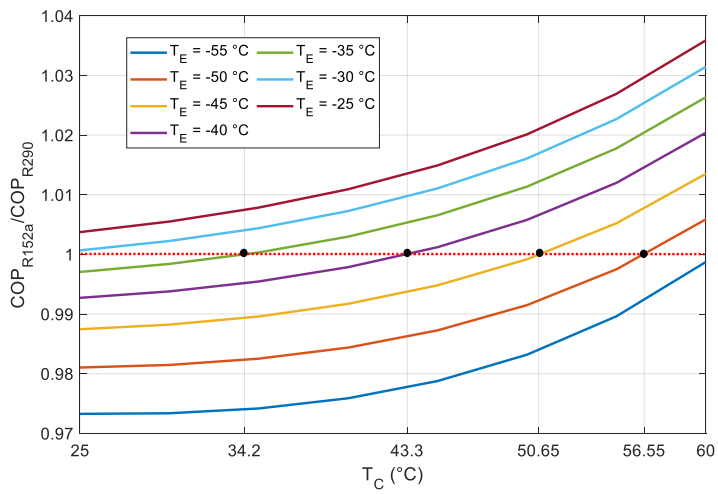

Note. Compiled by the authors

Figure 12

Compressor Power Consumption Ration Optimized

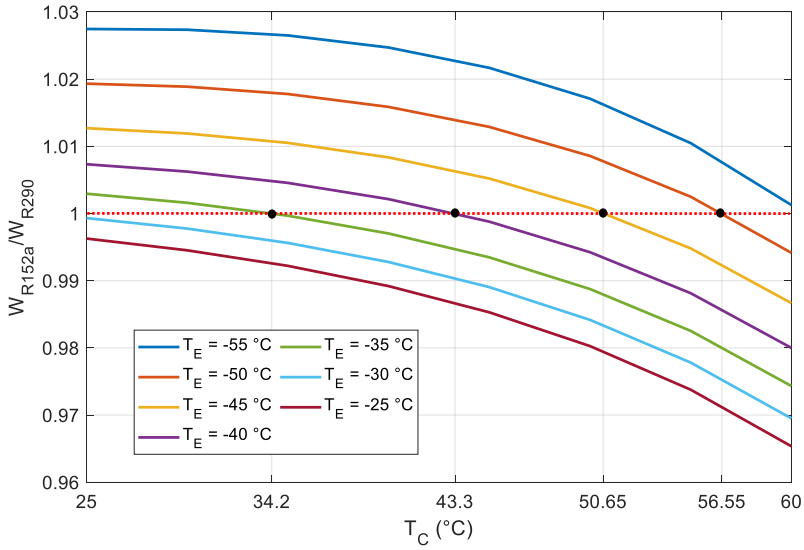

Note. Compiled by the authors

Figure 13

Exergy Destruction Ratio Optimized

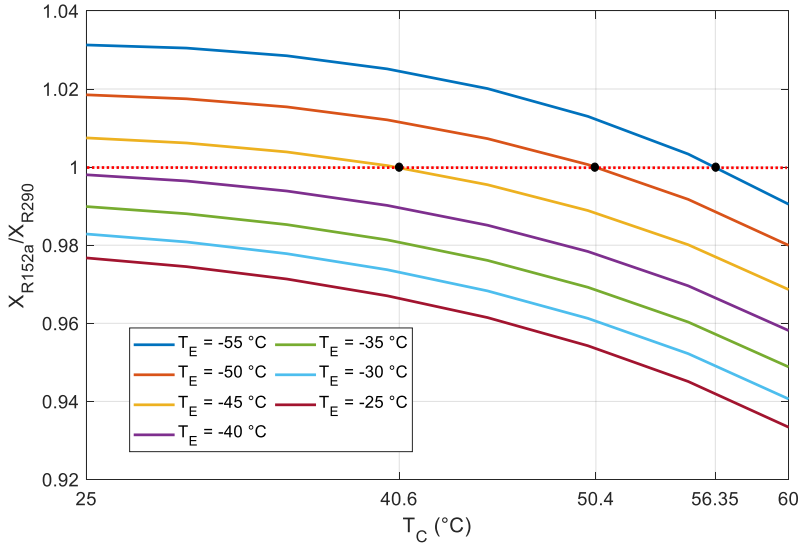

Note. Compiled by the authors

To evaluate the thermodynamic performance of the refrigeration system, the energy consumption, exergy destruction, and CO_2 equivalent production for the two refrigerant pairs are analysed and compared in the condensation temperature ranges from 25℃ to 60℃ and evaporation temperature ranges from -55℃ to -25℃. Figures 11 and 12 show the ratio between the coefficients of performance (COP) and the consumptions of the two systems (system operated with R744/R290 over system operated with R744/R152a), respectively. From this figure, the R744/R290 pair is better suited for very low evaporation temperatures, while the R744/R152a pair is well-suited for high evaporation temperatures. The ratio being equal to 1 means that the performances are identical. On the other hand, if the ratio is greater than 1, the performance of the system operating with the R744/R152a pair is better than the system

operated with R744/R290, and vice versa for ratios less than 1. In this light, we observe four remarkable condensation temperatures, namely $T_C = (34.2\,, 43.3\,, 50.65\,, 56.55)$°C. For these temperatures, the COPs are identical for $T_E = (-35\,, -40\,, -45\,, -50)$°C, respectively. Moreover, $COP_{R290}(T_E = -35) < COP_{R152a}(T_E = -35)$ for $T_C < 34.2$°C , $COP_{R290}(T_E = -40) < COP_{R152a}(T_E = -40)$, for $T_C < 43.3$°C, $COP_{R290}(T_E = -45) < COP_{R152a}(T_E = -45)$, for $T_C < 50.65$°C, $COP_{R290}(T_E = -50) < COP_{R152a}(T_E = -50)$ for $T_C < 56.55$°C and $COP_{R290}(T_E = -25) < COP_{R152a}(T_E = -25)$ for $T_C \in [25, 60]$°C, and for all value of T_C considered, $COP_{R290}(T_E = -55) > COP_{R152a}(T_E = -55)$.

Figure 14

TEWI Ratio Optimized

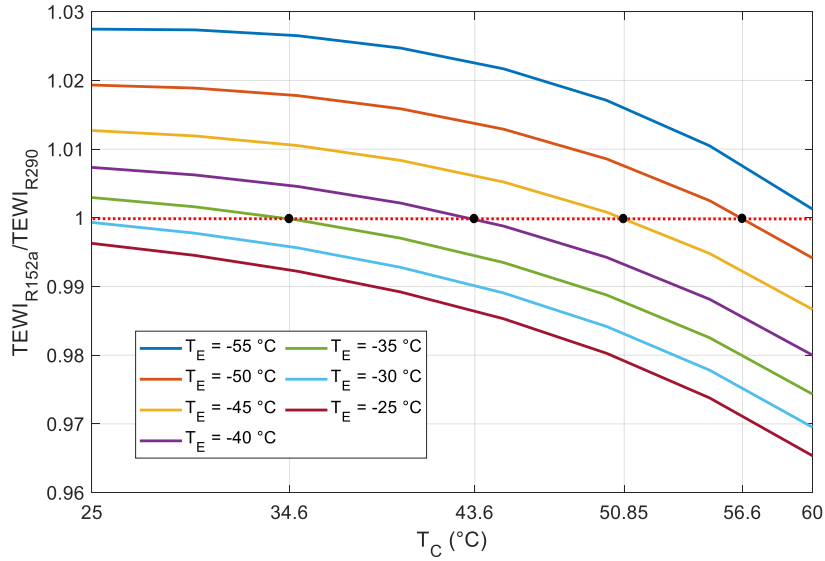

Note. Compiled by the authors

According to Figure 13, for a fixed T_C, when T_E increases, the destroyed exergy increases for each refrigerant group (Hamzaoui, Aidoun, et al., 2024). However, the increase varies from one pair to another. Figure 13 shows the evolution of the destroyed exergy ratios for the two considered refrigerant pairs. For $T_E \geq -40$°C, the ratio $X_{R152a}/X_{R290} < 1$, which shows that $X_{R152a} < X_{R290}$, thus the R744/R152a group is favored, while for $T_E = -45$°C, the R744/R290 pair is favoured for $T_C < 40.6$°C. On the other hand, if $T_C > 40.6$°C, then the R744/R152a group is better suited to be the operating group. Moreover, for $T_E = -50$°C and $T_E = -55$°C the R744/R152a pair is favoured in the intervals where $T_C < 50.4$°C and $T_C < 56.35$°C respectively. In all cases, this ratio increases with the decrease of T_E and T_C, thus increases with the increase of the difference $T_C - T_E$. Although the refrigerants used have GWPs < 150 (environmentally friendly), the carbon emissions of the two groups are calculated and analysed for optimal operation in the considered condensation and evaporation temperature ranges. The detailed variations of TEWI ratios between the R744/R152a and R744/R290 groups are presented in Figure 14. For the considered lifetime, it is easy to see the existence of condensation temperatures that mark the equality between the TEWIs of the two refrigerant pairs. From an environmental point of view, the R744/R290 pair is favoured for $T_E = -55$°C because the ratio $TEWI_{R152a}/TEWI_{R290} > 1$ regardless of the condensation temperature, while for $T_E > -30$°C, the R744/R152a pair is favored because the ratio $TEWI_{R152a}/TEWI_{R290} < 1$ regardless of the condensation temperature.

7. Regression functions

To predict the optimal (T_{4H}) within the operational range of the refrigeration cascade, multivariable regression models were developed to provide simple yet accurate correlations. Based on the results of the optimization procedure, an empirical function was formulated, allowing (T_{4H}) to be determined directly from the system's evaporation and condensation temperatures. This approach simplifies the determination of the optimal (T_{4H}) while maintaining high prediction accuracy within the considered operating range, making it particularly suitable for design and performance analysis of refrigeration cascades.

$$T_{4H-opt}(T_C, T_E) = a_0 + a_1 T_C + a_2 T_E + a_3 \frac{T_E}{T_C - T_E} \tag{32}$$

where T_C *and* T_E in ℃ and a_i $(i = 1, 2, 3, 4)$ are constants. (33)

Table 8 displays the values of the constants a_i in equation (28) for the two refrigerant pairs.

Table 8

Coefficients of Regression Functions

	a_0	a_1	a_2	a_3
R744/R290	-18.2876	0.4830	0.3797	1.3152
R744/R152a	-21.6878	0.4972	0.2861	1.6488

Note. Compiled by the authors

Figure 15

Comparison between T_{4H-OPT} Regression Function and Values of T_{4H-OPT} for CO_2/R290 Pair

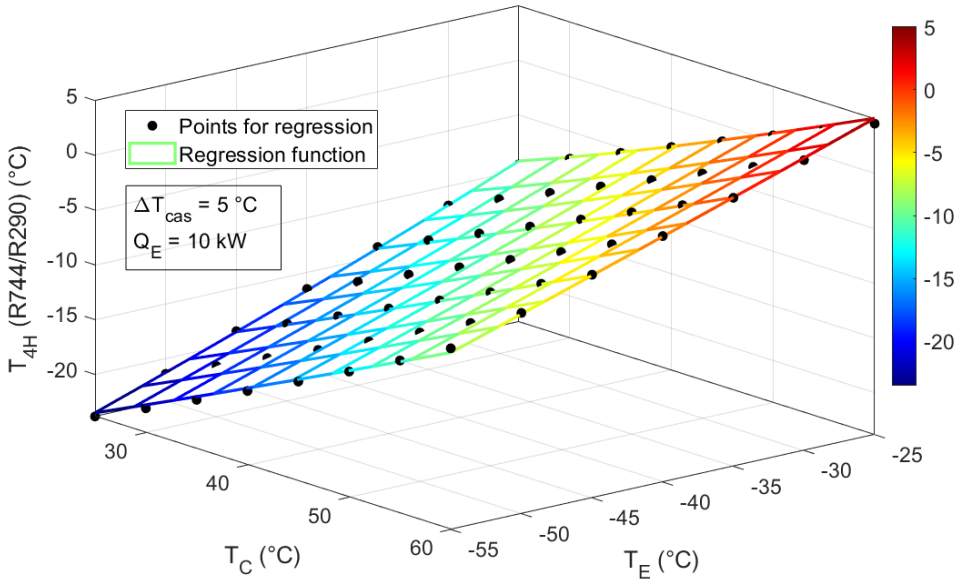

Note. Compiled by the authors

Equation (28) plays a crucial role in optimizing the installation's performance, with R^2 values exceeding 99.99% for the two considered groups of refrigerants. The RMSE and RRMSE values are less than 0.020 and 0.5%, respectively, indicating a highly satisfactory optimization score (see Figure 15 and 16). Furthermore, using equation (28) allows for the rapid determination of T_{4H-OPT}, providing control flexibility for optimal overall system operation.

8. Conclusion

Cascade refrigeration systems are combinations of two single-stage vapour compression refrigeration systems, typically used to achieve very low temperatures. In this series of single-stage vapour compression systems, thermally coupled at the HTC evaporator and LTC condenser, this combination is known as a cascade.

Figure 16

Comparison between T_{4H-OPT} Regression Function and Values of T_{4H-OPT} for CO_2/R152a Pair

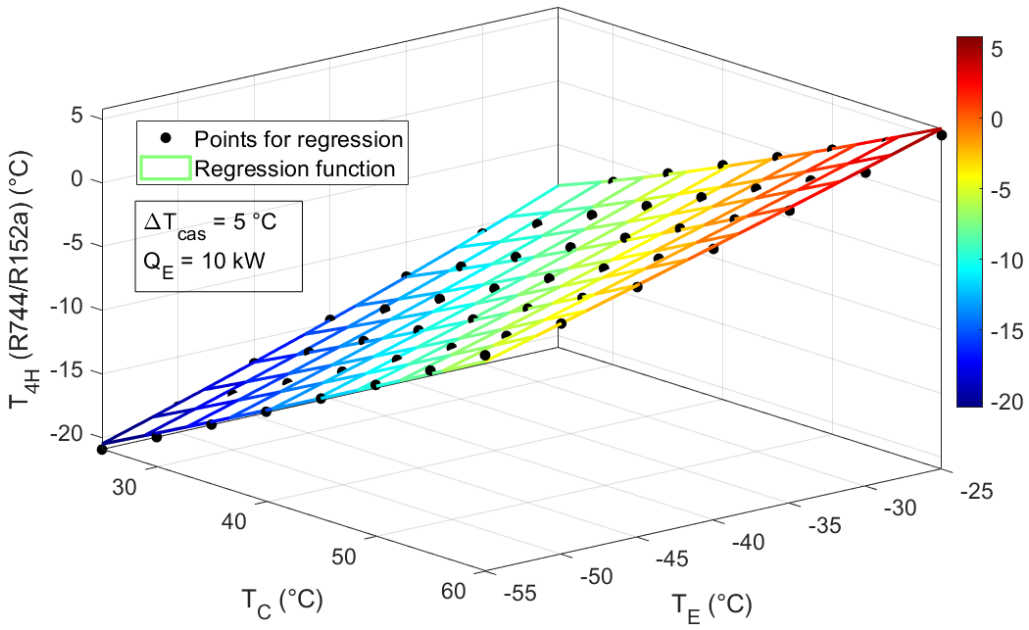

Note. Compiled by the authors

This system is designed to reach temperatures below $-25℃$ for various applications. The working fluids in the system are CO_2 (R744) in the LT loop and refrigerants R290 (C3H8) and R152a for the HT loop. These refrigerants are environmentally friendly, with their $GWP < 150$ and $ODP = 0$. The optimisation results show that:

- The R744/R290 pair is favoured for $T_E = -55℃$, while the R744/R152a pair is favored for $T_E \geq -30℃$, regardless of the condensation temperature.
- Between $T_E = -30℃$ and $T_E = -60℃$, there are condensation temperatures where the performance is identical, namely $T_C = (34.2\,, 43.3\,, 50.65\,, 56.55)℃$. For these temperatures, the COPs are identical for $T_E = (-35\,, -40\,, -45\,, -50)℃$ respectively. More precisely, $COP_{R290}(T_E = -35) < COP_{R152a}(T_E = -35)$ for $T_C < 34.2℃$, $COP_{R290}(T_E = -40) < COP_{R152a}(T_E = -40)$ for $T_C < 43.3℃$, $COP_{R290}(T_E = -45) < COP_{R152a}(T_E = -45)$ for $T_C < 50.65℃$, and $COP_{R290}(T_E = -50) < COP_{R152a}(T_E = -50)$ for $T_C < 56.55℃$.
- From an environmental point of view and over the considered lifetime of the installation, the R744/R290 pair is favoured for $T_E = -55℃$, while the R744/R152a pair is favoured for $T_E \geq -30℃$, regardless of the condensation temperature.
- A regression function that gives the optimal value of T_{4H} is provided for use in controlling this type of installation.

SCIENTIFIC CONTRIBUTION

The manuscript extends or refines existing theories; the manuscript proposes a new theoretical or analytical model; the manuscript opens new directions for further research.

AUTHOR CONTRIBUTIONS

CRediT: **Malek Hamzaoui**: Methodology, Software, Validation, Formal Analysis, Writing - Original Draft, Writing - Review & Editing, Visualization, Supervision; **Samir Tiachacht**: Methodology, Software, Writing - Original Draft, Writing - Review & Editing, Visualization, Supervision; **Ali Grine**: Methodology, Writing - Original Draft; **Ahmed Hadiouche**: Writing - Original Draft.

FUNDING

This research received no external funding.

NO CONFLICT OF INTEREST STATEMENT

All authors declare that they have no conflict of interest.

References

Abdollahzadeh, B., Khodadadi, N., Barshandeh, S., Trojovský, P., Gharehchopogh, F. S., El-kenawy, E.-S. M., Abualigah, L., & Mirjalili, S. (2024). Puma optimizer (PO): A novel metaheuristic optimization algorithm and its application in machine learning. *Cluster Computing*, *27*(4), 5235-5283. https://doi.org/10.1007/s10586-023-04221-5

Adebayo, V., Abid, M., Adedeji, M., Dagbasi, M., & Bamisile, O. (2021). Comparative thermodynamic performance analysis of a cascade refrigeration system with new refrigerants paired with CO_2. *Applied Thermal Engineering*, *184*, Article 116286. https://doi.org/10.1016/j.applthermaleng.2020.116286

Bencharif, M., Nesreddine, H., Perez, S. C., Poncet, S., & Zid, S. (2020). The benefit of droplet injection on the performance of an ejector refrigeration cycle working with R245fa. *International Journal of Refrigeration*, *113*, 276-287. https://doi.org/https://doi.org/10.1016/j.ijrefrig.2020.01.020

Bhattacharyya, S., Garai, A., & Sarkar, J. (2009). Thermodynamic analysis and optimization of a novel N_2O-CO_2 cascade system for refrigeration and heating. *International Journal of Refrigeration*, *32*(5), 1077-1084. https://doi.org/10.1016/j.ijrefrig.2008.09.008

Cabello, R., Sánchez, D., Llopis, R., Catalán, J., Nebot-Andrés, L., & Torrella, E. (2017). Energy evaluation of R152a as drop in replacement for R134a in cascade refrigeration plants. *Applied Thermal Engineering*, *110*, 972-984. https://doi.org/10.1016/j.applthermaleng.2016.09.010

Davoodi, V., Kazemiani-Najafabadi, P., & Amiri Rad, E. (2022). Presenting a power and cascade cooling cycle driven using solar energy and natural gas. *Renewable Energy*, *186*, 802-813. https://doi.org/10.1016/j.renene.2022.01.031

de Paula, C. H., Duarte, W. M., Rocha, T. T. M., de Oliveira, R. N., & Maia, A. A. T. (2020). Optimal design and environmental, energy and exergy analysis of a vapor compression refrigeration system using R290, R1234yf, and R744 as alternatives to replace R134a. *International Journal of Refrigeration*, *113*, 10-20. https://doi.org/10.1016/j.ijrefrig.2020.01.012

Gado, M. G., Megahed, T. F., Ookawara, S., Nada, S., & El-Sharkawy, I. I. (2022). Potential application of cascade adsorption-vapor compression refrigeration system powered by photovoltaic/thermal collectors. *Applied Thermal Engineering*, *207*, Article 118075. https://doi.org/10.1016/j.applthermaleng.2022.118075

Hamzaoui, M., Aidoun, Z., Nesreddine, H., & Tiachacht, S. (2024). Optimisation of a cascade refrigeration system with natural refrigerants, based on nature-inspired algorithms. *Arabian Journal for Science and Engineering*, *49*(5), 7701-7730. https://doi.org/10.1007/s13369-023-08689-6

Hamzaoui, M., Nesreddine, H., Aidoun, Z., & Balistrou, M. (2018). Experimental study of a low grade heat driven ejector cooling system using the working fluid R245fa. *International Journal of Refrigeration*, *86*, 388-400. https://doi.org/10.1016/j.ijrefrig.2017.11.018

Hamzaoui, M., Tiachacht, S., & Hadiouche, A. (2024). Optimization of a three-stage cascade refrigeration system operating with natural refrigerants to produce low temperatures by applying a bio-inspired method. *Thermal Science and Engineering Progress*, *50*, Article 102519. https://doi.org/10.1016/j.tsep.2024.102519

Han, X. H., Wang, Q., Zhu, Z. W., & Chen, G. M. (2007). Cycle performance study on R32/R125/R161 as an alternative refrigerant to R407C. *Applied Thermal Engineering*, *27*(14), 2559-2565. https://doi.org/10.1016/j.applthermaleng.2007.01.034

Houssein, E. H., Oliva, D., Samee, N. A., Mahmoud, N. F., & Emam, M. M. (2023). Liver cancer algorithm: A novel bio-inspired optimizer. *Computers in Biology and Medicine*, *165*, Article 107389. https://doi.org/10.1016/j.compbiomed.2023.107389

Kilicarslan, A., & Hosoz, M. (2010). Energy and irreversibility analysis of a cascade refrigeration system for various refrigerant couples. *Energy Conversion and Management*, *51*(12), 2947-2954. https://doi.org/10.1016/j.enconman.2010.06.037

Kumar, S., Gahlot, P., & Kumar, S. (2024). Energy, exergy and economical analysis of N_2O based cascade refrigeration system for ultralow temperature cooling applications using different eco-friendly refrigerants in high temperature cycle. *Results in Engineering*, *22*, Article 102259. https://doi.org/10.1016/j.rineng.2024.102259

Kumar, S., Gahlot, P., & Kumar, S. (2026). Energy, exergy, environmental, and economical (4E) analysis of modified cascade refrigeration cycles for ultra-low temperature cooling applications. *Journal of Thermal Analysis and Calorimetry*. Advance online publication. https://doi.org/10.1007/s10973-025-15249-7

Lemmon, E. W., Huber, M. L., & McLinden, M. O. (2007). *NIST standard reference database 23: Reference fluid thermodynamic and transport properties-REFPROP, version 8.0*. National Institute of Standards and Technology.

Liu, X., Li, J., Hou, K., Wang, S., & He, M. (2022). New environment friendly working pairs of dimethyl ether and ionic liquids for absorption refrigeration with high COP. *International Journal of Refrigeration*, *134*, 159-167. https://doi.org/10.1016/j.ijrefrig.2021.11.031

Lizarte, R., Palacios-Lorenzo, M. E., & Marcos, J. D. (2017). Parametric study of a novel organic Rankine cycle combined with a cascade refrigeration cycle (ORC-CRS) using natural refrigerants. *Applied Thermal Engineering*, *127*, 378-389. https://doi.org/10.1016/j.applthermaleng.2017.08.063

Logesh, K., Baskar, S., Azeemudeen, M., Praveen Reddy, B., & Venkata Subba Sai Jayanth, G. (2019). Analysis of cascade vapour refrigeration system with various refrigerants. *Materials Today: Proceedings*, *18*, 4659-4664. https://doi.org/10.1016/j.matpr.2019.07.450

Ma, X., Fang, Y., Dai, Q., He, Z., Yang, J., Liu, J., & Zou, H. (2025). Experimental evaluation of a high temperature cascade heat pump based on refrigerant charge. *Case Studies in Thermal Engineering*, *73*, Article 106573. https://doi.org/10.1016/j.csite.2025.106573

Mirjalili, S. (2015). The Ant Lion optimizer. *Advances in Engineering Software*, *83*, 80-98. https://doi.org/10.1016/j.advengsoft.2015.01.010

Nesreddine, H., Bendaoud, A., Aidoun, Z., Ouzzane, M., & Le Lostec, B. (2015, August 16-22). *Experimental investigation of an ejector-compression cascade system activated with low-grade waste heat* [Paper presentation]. 24th IIR International Congress of Refrigeration, Yokohama, Japan.

Pektezel, O., & Ozdemir, S. N. (2025). Performance optimization of new generation R290 and R1234yf refrigerants: A response surface methodology approach. *Applied Thermal Engineering*, *269*, Article 125927. https://doi.org/10.1016/j.applthermaleng.2025.125927

Salhi, K., Korichi, M., & Ramadan, K. M. (2018). Thermodynamic and thermo-economic analysis of compression-absorption cascade refrigeration system using low-GWP HFO refrigerant powered by geothermal energy. *International Journal of Refrigeration*, *94*, 214-229. https://doi.org/10.1016/j.ijrefrig.2018.03.017

Sun, Z., Liang, Y., Liu, S., Ji, W., Zang, R., Liang, R., & Guo, Z. (2016). Comparative analysis of thermodynamic performance of a cascade refrigeration system for refrigerant couples R41/R404A and R23/R404A. *Applied Energy*, *184*, 19-25. https://doi.org/10.1016/j.apenergy.2016.10.014

Sun, Z., Wang, Q., Xie, Z., Liu, S., Su, D., & Cui, Q. (2019). Energy and exergy analysis of low GWP refrigerants in cascade refrigeration system. *Energy*, *170*, 1170-1180. https://doi.org/10.1016/j.energy.2018.12.055

Udroiu, C.-M., Giménez-Prades, P., Navarro-Esbrí, J., Barragán-Cervera, Á., & Mota-Babiloni, A. (2025). Experimental evaluation of a two-stage cascade ultra-low temperature refrigeration system with internal heat exchanger using hydrocarbon pair R290/R170 and comparison with HFC baseline. *Applied Thermal Engineering*, *274*, Article 126679. https://doi.org/10.1016/j.applthermaleng.2025.126679

Ye, W., Liu, Y., Yan, Y., Hu, L., Su, M., & Liu, Y. (2026). Performance analysis and enhancement of cascade refrigeration systems through multi-objective grey wolf optimization algorithm. *Thermal Science and Engineering Progress*, *70*, Article 104504. https://doi.org/https://doi.org/10.1016/j.tsep.2026.104504

Zhao, W., Wang, L., Zhang, Z., Mirjalili, S., Khodadadi, N., & Ge, Q. (2023). Quadratic Interpolation Optimization (QIO): A new optimization algorithm based on generalized quadratic interpolation and its applications to real-world engineering problems. *Computer Methods in Applied Mechanics and Engineering*, *417*, Article 116446. https://doi.org/10.1016/j.cma.2023.116446

APPENDIX

Nomenclature

h :	Enthalpy (kJ/kg)	$\dot{Q}$:	Heat flow rate (kW)
$\dot{m}$:	Mass flow rate (kg/s)	s :	Entropie (kJ/kg.K)
NBT :	Normal boiling temperature (°C)	T :	Temperature (K)
P :	Pressure (bar)	$\dot{W}$:	Power (kW)
$TEWI$:	Total Equivalent Warming Impact ($kgCO_2eq$)		
$\dot{X}_i$:	Exergy destruction for i component (kW)		

Note. Complied by the authors

Greek Letters

Δ :	Difference	τ_c :	Compression ratio
η :	Efficiency	ε :	Heat exchanger efficiency

Note. Complied by the authors

Acronyms

ALO :	Ant Lion Optimizer	LCA :	Liver Cancer Algorithm.
COP :	Coefficient of performance	ODP :	Ozone depletion potential
GWP :	Global warming potential	Puma :	Puma optimizer
QIO :	Quadratic Interpolation Optimization		
$TEWI$:	Total equivalent warming impact		

Note. Complied by the authors

Subscripts

0 :	Reference	is :	Isentropic
1L ... 1sL :	State points of LT cycle	C :	Condenser
1H ... 1sH :	State points of HT cycle	cas :	Cascade
cr :	Critical point	LTC :	Low-temperature cycle
DIR :	Direct	rH :	Sub-cooled of HT cycle
E :	Evaporator	rL :	Sub-cooled of LT cycle
EXV :	Expansion valve	sH :	Super-heated of HT cycle
HTC :	high-temperature cycle	sL :	Super-heated of LT cycle
$IESHT$:	HTC internal heat exchanger	VHT :	HT expansion valve
$IESLT$:	HTC internal heat exchanger	VLT :	LT expansion valve
IND :	Indirect		

Note. Complied by the authors

© 2026 The Author(s). Published by HCMCOU Journal of Science - Advances in Computational Structures. This article is licensed under CC BY-NC 4.0.